Efficient high order semi-implicit time discretization and local discontinuous Galerkin methods for highly nonlinear PDEs

Ruihan Guo[*], Francis Filbet[†], Yan Xu[‡]

Abstract

In this paper, we develop a high order semi-implicit time discretization method for highly nonlinear PDEs, which consist of the surface diffusion and Willmore flow of graphs, the Cahn-Hilliard equation and the Allen-Cahn/Cahn-Hilliard system. These PDEs are high order in spatial derivatives, which motivates us to develop implicit or semi-implicit time marching methods to relax the severe time step restriction for stability of explicit methods. In addition, these PDEs are also highly nonlinear, fully implicit method will incredibly increase the difficulty of implementation. In particular, we can not well separate the stiff and non-stiff components for these problems, which leads to the traditional implicit-explicit methods nearly meaningless. In this paper, a high order semi-implicit time marching method and the local discontinuous Galerkin spatial method are coupled together to achieve high order accuracy in both space and time, and to enhance the efficiency of the proposed approaches, the resulting linear or nonlinear algebraic systems are solved by multigrid solver. Numerical simulation results in one and two dimensions are presented to illustrate that the combination of the local discontinuous Galerkin method for spatial approximation, semi-implicit temporal integration with the multigrid solver provides a practical and efficient approach when solving this family of problems.

[*]Institut Camille Jordan, Université Claude Bernard Lyon I, 43 boulevard 11 novembre 1918, 69622 Villeurbanne cedex, France. Email: rguo@math.univ-lyon1.fr.

[†]Institut de Mathématiques de Toulouse, Université Paul Sabatier Toulouse III, 118 route de Narbonne, 31062 Toulouse cedex, France. Email: francis.filbet@math.univ-toulouse.fr.

[‡]School of Mathematical Sciences, University of Science and Technology of China, Hefei, Anhui 230026, P.R. China. Email: yxu@ustc.edu.cn.

Key words: semi-implicit time marching method, local discontinuous Galerkin method, multigrid, surface diffusion and Willmore flow of graphs, Cahn-Hilliard equation, Allen-Cahn/Cahn-Hilliard system

1 Introduction

In this paper, we consider efficient high order semi-implicit time discretization and the local discontinuous Galerkin (LDG) method for time dependent highly nonlinear partial differential equations (PDEs) containing high order spatial derivatives.

The discontinuous Galerkin (DG) method is a class of finite element methods, in which using a completely discontinuous piecewise polynomials as the numerical solution and the test spaces. Reed and Hill [14] first designed it as a method for solving first order linear transport equation. Cockburn *et al.* later extended the DG method to solve nonlinear hyperbolic conservation laws in a series of papers [3, 4, 5, 6].

It is difficult to apply the DG method directly to PDEs containing higher order spatial derivatives, therefore the LDG method was introduced. The idea of the LDG method is to rewrite the equations with higher order derivatives as a first order system, then apply the DG method to the system. The first LDG method was constructed by Cockburn and Shu in [7] for solving a convection diffusion equation (containing second derivatives). Their work was motivated by the successful numerical experiments of Bassi and Rebay [1] for the compressible Navier-Stokes equations. For a detailed description about the LDG methods for high order time-dependent PDEs, we refer the readers to the review paper [22]. A common feature of these LDG methods is that stability can be proved for quite general nonlinear cases. DG and LDG methods also have several attractive properties, such as easy parallelization, easy adaptivity and simple treatment of boundary conditions. The most important property of DG and LDG methods is high order accuracy, which motivates us to develop high order temporal accuracy scheme to get the goal of obtaining high order accuracy in both space and time.

By the method of lines, the application of the LDG method for spatial variables for a partial differential equation will generate a large coupled system of ordinary differential equations (ODEs). The development of a suitable ODEs solver attracted a lot of attention in the last decades. Explicit high order nonlinearly stable Runge-Kutta methods are efficient for hyperbolic problems or convection dominated problems. However, if the PDEs contain

high order spatial derivatives with coefficients not very small, then explicit temporal methods suffer from severe time step restrictions for stability, of the form $\Delta t \leqslant C\Delta x^p$, where p is the order of the PDE. It would therefore be desirable to develop implicit or semi-implicit time discretization techniques to alleviate this problem, especially for long time simulations.

In [18], three different time discretization techniques for solving the stiff ODEs resulting from an LDG spatial discretization to PDEs with higher order spatial derivatives were explored. These are the semi-implicit spectral deferred correction (SDC) method, the additive Runge-Kutta (ARK) method and the exponential time differencing (ETD) method, which are all validated to be efficient. However, these three methods are mainly efficient for a problem with easily separate stiff and non-stiff components, which treating the non-stiff terms explicitly and the stiff terms implicitly. Actually, it is not always easy to separate stiff and non-stiff components, for example, for the surface diffusion and Willmore flow of graphs, the Cahn-Hilliard equation with degenerate mobility and the Allen-Cahn/Cahn-Hilliard system with degenerate mobility, which are all highly nonlinear and containing higher order spatial derivatives. In such cases, one usually relies on fully implicit schemes. However, fully implicit schemes have the disadvantage of difficult implementation and poor stability properties, especially for fully nonlinear problems.

The surface diffusion and Willmore flow of graphs are both highly nonlinear fourth-order PDEs. Smereka [15] developed a splitting technique for the surface diffusion of graphs, which was effective to stabilize numerical schemes but it may affect the numerical accuracy. In [8], a first order semi-implicit numerical scheme for the Willmore flow of graphs based on a finite element method was presented. Various unconditionally stable first order [10, 11] temporal discretization schemes have been developed for the Cahn-Hilliard equation, based on the convex splitting technique. These schemes are only first order accurate, and for the Cahn-Hilliard equation with constant mobility, it is easy to extend to higher order accurate ones by the methods introduced in [20], but for the Cahn-Hilliard equation with degenerate mobility, high order temporal schemes are very difficult to derive. There have been limited numerical simulations works in the existing literature for efficient semi-implicit time marching method for solving the Allen-Cahn/Cahn-Hilliard system, and it would therefore be desirable to develop high order semi-implicit schemes for the system.

In this paper, we focus on high order semi-implicit time marching methods for PDEs with high order spatial derivatives and highly nonlinear, *i.e.* the stiff and non-stiff components can not be well separated. Coupled with the LDG spatial discretization, we will construct a

semi-implicit fully discrete scheme for the surface diffusion and Willmore flow of graphs, the Cahn-Hilliard equation with degenerate mobility and the Allen-Cahn/Cahn-Hilliard system, which is high order accurate in both space and time. Obviously, it requires to solve system of linear or nonlinear equations at each time step. Traditional iterative solution methods such as Gauss-Seidel method suffers from slow convergence rates, especially for larger system. To enhance the efficiency of the proposed approach, the multigrid solver is employed to solve the algebraic equations at each time step.

The outline of this paper is as follows. In Section 2, we give a description of the high order semi-implicit time marching method. Section 3 is devoted to the application of LDG method and the semi-implicit time marching method for a series of highly nonlinear PDEs with higher order spatial derivatives. Numerical examples are also presented, testing the performance of the time marching method coupled with the LDG spatial discretization for these PDEs, including the surface diffusion and Willmore flow of graphs, the Cahn-Hilliard equation with degenerate mobility and the Allen-Cahn/Cahn-Hilliard system. Finally we give concluding remarks in Section 4.

2 The high order semi-implicit time marching method

The surface diffusion and Willmore flow of graphs, the Cahn-Hilliard equation and the Allen-Cahn/Cahn-Hilliard system are all PDEs of highly nonlinear, and the stiff and non-stiff components for these problems can not be well separated. After the LDG spatial discretization for these problems, we can get an ODEs of the form

$$\begin{cases} \dfrac{du}{dt}(t) = \mathcal{H}(t, u(t), u(t)), \\ u(t_0) = u_0, \end{cases} \tag{2.1}$$

where $m \in \mathbb{N}$, $u(t) \in \mathbb{R}^m$, $\mathcal{H} : \mathbb{R} \times \mathbb{R}^m \times \mathbb{R}^m \to \mathbb{R}^m$ and $\mathcal{H} \in C^1(\mathbb{R} \times \mathbb{R}^m \times \mathbb{R}^m)$, and the dependence on the second argument of $\mathcal{H}$ is non-stiff, while the dependence on the third argument is stiff. In this section, we will devote to developing a high order semi-implicit time marching method to solve (2.1).

2.1 The partitioned Runge-Kutta methods

Boscarino *et al.* presented a new class of semi-implicit Runge-Kutta methods in [2], which was based on the partitioned Runge-Kutta methods. Therefore, in order to introduce the

semi-implicit Runge-Kutta method, we will first give a simple description for the partitioned Runge-Kutta methods. We consider autonomous differential equations in the partitioned form,

$$\begin{cases} \dfrac{dy}{dt}(t) = \mathcal{F}(y(t), z(t)), \\ \dfrac{dz}{dt}(t) = \mathcal{G}(y(t), z(t)), \end{cases} \tag{2.2}$$

where $y(t) \in \mathbb{R}^m$, $z(t) \in \mathbb{R}^n$, $\mathcal{F} : \mathbb{R}^m \times \mathbb{R}^n \to \mathbb{R}^m$, $\mathcal{G} : \mathbb{R}^m \times \mathbb{R}^n \to \mathbb{R}^n$ and $\mathcal{F}, \mathcal{G} \in \mathcal{C}^1(\mathbb{R}^m \times \mathbb{R}^n)$, which are sufficient to guarantee local existence and uniqueness of the solution to (2.2). $y(t_0) = y_0$, $z(t_0) = z_0$ are the initial conditions.

Then we can express the partitioned Runge-Kutta methods by applying two different Runge-Kutta methods as the following Butcher tableau:

$$\begin{array}{c|c} \hat{c} & \hat{A} \\ \hline & \hat{b}^T \end{array} \qquad\qquad \begin{array}{c|c} c & A \\ \hline & b^T \end{array}$$

In the above tableau, the pair $(\hat{A}|\hat{b})$ determines explicit Runge-Kutta methods and $(A|b)$ defines implicit Runge-Kutta methods, which means that the first variable $y(t)$ is treated by explicit method and the second variable $z(t)$ is treated by implicit method. The Butcher coefficients $\hat{A} = (\hat{a}_{i,j})$, $A = (a_{i,j}) \in \mathbb{R}^{s\times s}$, $\hat{b}^T = (\hat{b}_1, \ldots, \hat{b}_s)$, $b^T = (b_1, \ldots, b_s)$, $\hat{c} = (\hat{c}_1, \ldots, \hat{c}_s)$ and $c = (c_1, \ldots, c_s)$ are constrained by order of accuracy and stability considerations.

For practical reasons, in order to simplify the computations, we consider that $\hat{A}$ is a strictly lower triangular matrix and $\hat{A}$ is a lower triangular matrix for the implicit part. In addition, the coefficients satisfy:

$$\hat{c}_i = \sum_{j=1}^{i-1} \hat{a}_{i,j}, \quad \text{and} \quad c_i = \sum_{j=1}^{i} a_{i,j}, \quad \text{for} \quad 1 \leqslant i \leqslant s. \tag{2.3}$$

By applying the partitioned Runge-Kutta time marching method, the solution of the autonomous system (2.2) advanced from time t^n to $t^{n+1} = t^n + \Delta t$ is given by

$$\begin{cases} k_i = \mathcal{F}\left(y^n + \Delta t \sum_{j=1}^{i-1} \hat{a}_{i,j}\, k_j,\; z^n + \Delta t \sum_{j=1}^{i} a_{i,j}\, l_j \right), \quad 1 \leqslant i \leqslant s, \\ l_i = \mathcal{G}\left(y^n + \Delta t \sum_{j=1}^{i-1} \hat{a}_{i,j}\, k_j,\; z^n + \Delta t \sum_{j=1}^{i} a_{i,j}\, l_j \right), \quad 1 \leqslant i \leqslant s, \end{cases} \tag{2.4}$$

and we can calculate y^{n+1} and z^{n+1} as follows

$$\begin{cases} y^{n+1} \;=\; y^n \;+\; \Delta t \sum_{i=1}^{s} \hat{b}_i \, k_i, \\ \\ z^{n+1} \;=\; z^n \;+\; \Delta t \sum_{i=1}^{s} b_i \, l_i. \end{cases} \tag{2.5}$$

2.2 The semi-implicit Runge-Kutta methods

After an overview of the partitioned Runge-Kutta methods, we will pay special attention to the high order semi-implicit Runge-Kutta methods in this subsection. Our goal is to develop a high order semi-implicit time marching method for equation (2.1), but not fully implicit scheme. To derive a semi-implicit Runge-Kutta scheme, we first rewrite the non autonomous differential equation (2.1) as an autonomous system where we double the number of variable, that is,

$$\begin{cases} \dfrac{d}{dt} \begin{pmatrix} t \\ u(t) \end{pmatrix} \;=\; \begin{pmatrix} 1 \\ \mathcal{H}(t, u(t), u(t)) \end{pmatrix}, \\ \\ \dfrac{du(t)}{dt} \qquad\quad = \mathcal{H}(t, u(t), u(t)). \end{cases} \tag{2.6}$$

This system now corresponds to an autonomous partitioned system (2.4), with $y(t) = (t, u(t))$, $\mathcal{F} = (1, \mathcal{H})$ and $z(t) = u(t)$, $\mathcal{G} = \mathcal{H}$ and $y(t_0) = (t_0, u_0)$, $z(t_0) = u_0$ are the initial conditions. Applying the partitioned Runge-Kutta scheme (2.4)-(2.5) to system (2.6), we can get a high order semi-implicit Runge-Kutta method for (2.1) : the first component of the first equation (2.6) only gives

$$\hat{c}_i = \sum_{j=1}^{i} \hat{a}_{i,j},$$

whereas the second component of the first equation and the second equation of (2.6) gives the semi-implicit scheme

$$k_i = \mathcal{H}\left(t^n + \hat{c}_i \Delta t, u^n \;+\; \Delta t \sum_{j=1}^{i-1} \hat{a}_{i,j} \, k_j, u^n \;+\; \Delta t \sum_{j=1}^{i} a_{i,j} \, k_j \right), \quad 1 \leqslant i \leqslant s.$$

Therefore, starting from u^n, we give the algorithm to calculate u^{n+1} in the following.

1. Set for $i = 1, \ldots, s$,

$$U_i = u^n + \Delta t \sum_{j=1}^{i-1} \hat{a}_{i,j} k_j,$$

$$V_i = u^n + \Delta t \sum_{j=1}^{i} a_{i,j} k_j. \tag{2.7}$$

2. For $i = 1, \ldots, s$, compute

$$k_i = \mathcal{H}(t^n + \hat{c}_i \Delta t, U_i, V_i). \tag{2.8}$$

3. Update the numerical solution u^{n+1} as

$$u^{n+1} = u^n + \Delta t \sum_{i=1}^{s} b_i \, k_i. \tag{2.9}$$

By algorithm (2.7)-(2.9), the second variable of equation (2.1) is treated explicitly and the third one is treated implicitly. Obviously, it is necessary to solve system of linear or nonlinear algebraic equations (2.8) at each time step. The overall performance highly depends on the performance of the solver. Traditional iterative solution methods such as Gauss-Seidel method suffers from slow convergence rates, especially for large systems. To enhance the efficiency of the high order semi-implicit time marching method, we will apply the multigrid solver to solve algebraic equations (2.8) in this paper. And for a detailed description of the multigrid solver, we refer the readers to Trottenberg *et al.* [16].

In this paper, we focus on a second order L-stable scheme and a third order one. The second order L-stable is given in the following form

$$\begin{array}{c|cc} 0 & 0 & 0 \\ 1 & 1 & 0 \\ \hline & 1/2 & 1/2 \end{array} \qquad \begin{array}{c|cc} \gamma & \gamma & 0 \\ 1-\gamma & 1-2\gamma & \gamma \\ \hline & 1/2 & 1/2 \end{array}$$

with $\gamma = 1 - 1/\sqrt{2}$. While for the third order L-stable scheme, the corresponding Butcher tableau is given by

$$\begin{array}{c|cccc} 0 & 0 & 0 & 0 & 0 \\ 0 & 0 & 0 & 0 & 0 \\ 1 & 0 & 1 & 0 & 0 \\ 1/2 & 0 & 1/4 & 1/4 & 0 \\ \hline & 0 & 1/6 & 1/6 & 2/3 \end{array} \qquad \begin{array}{c|cccc} \alpha & \alpha & 0 & 0 & 0 \\ 0 & -\alpha & \alpha & 0 & 0 \\ 1 & 0 & 1-\alpha & \alpha & 0 \\ 1/2 & \beta & \eta & 1/2-\beta-\eta-\alpha & \alpha \\ \hline & 0 & 1/6 & 1/6 & 2/3 \end{array}$$

with $\alpha = 0.24169426078821$, $\beta = \alpha/4$ and $\eta = 0.12915286960590$.

3 Applications of LDG method and semi-implicit time marching methods

In this section, we perform numerical experiments of the LDG scheme coupled with the proposed high order semi-implicit time marching method for the surface diffusion of graphs, the Willmore flow of graphs, the Cahn-Hilliard equation and the Allen-Cahn/Cahn-Hilliard system . To enhance the efficiency of the proposed approach, the multigrid solver is used to solve the algebraic equations at each time step. We present some accuracy tests to show that the proposed spatial and time discretization methods can achieve high order accuracy in both space and time. Then we will show some long time simulations. All the computations are performed in double precision and on uniform spatial meshes.

3.1 The surface diffusion and Willmore flow of graphs

In this subsection, we consider LDG spatial discretization coupled with high order semi-implicit Runge-Kutta method (2.7)-(2.9) for the surface diffusion of graphs

$$u_t + \nabla \cdot \left(Q \left(\boldsymbol{I} - \frac{\nabla u \otimes \nabla u}{Q^2} \right) \nabla H \right) = 0 \tag{3.10}$$

and Willmore flow of graphs

$$u_t + Q\nabla \cdot \left(\frac{1}{Q} \left(\boldsymbol{I} - \frac{\nabla u \otimes \nabla u}{Q^2} \right) \nabla (QH) \right) - \frac{1}{2} Q \nabla \cdot \left(\frac{H^2}{Q} \nabla u \right) = 0, \tag{3.11}$$

where Q is the area element

$$Q = \sqrt{1 + |\nabla u|^2} \tag{3.12}$$

and H is mean curvature of the domain boundary Γ

$$H = \nabla \cdot \left(\frac{\nabla u}{Q} \right). \tag{3.13}$$

Xu and Shu [21] developed the LDG finite element methods for these two equations, which were high order accuracy in space. However, the forward Euler method was applied for time discretization with a suitably small time step Δt ($\Delta t = O(\Delta x^4)$) for stability, which was not efficient, especially for long time simulations. These two equations are both highly nonlinear, which increases the difficulty of developing semi-implicit time marching method, not to mention high order scheme. To achieve high order accuracy in time, we will apply the proposed semi-implicit Runge-Kutta method (2.7)-(2.9) to these two equations.

After the LDG spatial discretization, we can apply our semi-implicit Runge-Kutta scheme by writing the ODEs in the form (2.1) with u the component treated explicitly, v the component treated implicitly and

$$\mathcal{H}(t,u,v) = -\nabla\cdot\left(Q(u)\left(\boldsymbol{I}-\frac{\nabla u\otimes\nabla u}{Q(u)^2}\right)\nabla H(u,v)\right) \tag{3.14}$$

for surface diffusion of graphs (3.10), where

$$Q(u)=\sqrt{1+|\nabla u|^2},\quad \text{and}\quad H(u,v)=\nabla\cdot\left(\frac{\nabla v}{Q(u)}\right). \tag{3.15}$$

While for Willmore flow of graphs (3.11), $\mathcal{H}$ is given as

$$\mathcal{H}(t,u,v) = -Q(u)\nabla\cdot\left(\frac{1}{Q(u)}\left(\boldsymbol{I}-\frac{\nabla u\otimes\nabla u}{Q(u)^2}\right)\nabla(Q(u)H(u,v))\right)+\frac{1}{2}Q(u)\nabla\cdot\left(\frac{H(u)^2}{Q(u)}\nabla v\right), \tag{3.16}$$

where

$$Q(u)=\sqrt{1+|\nabla u|^2},\quad \text{and}\quad H(u,v)=\nabla\cdot\left(\frac{\nabla v}{Q(u)}\right)\quad \text{and}\quad H(u)=\nabla\cdot\left(\frac{\nabla u}{Q(u)}\right). \tag{3.17}$$

With the proposed space and time discretization methods, we will achieve a high order scheme in both space and time with a larger time step, *i.e.* $\Delta t = O(\Delta x)$. Next we will present some numerical experiments to validate the result.

Example 3.1. Accuracy test for surface diffusion of graphs

In this example, we consider the accuracy test for one-dimensional surface diffusion of graphs. We test our method taking the exact solution

$$u(x,t) = 0.05\cos(t)\sin(x) \tag{3.18}$$

for equation (3.10) with a source term f, which is a given function so that (3.18) is the exact solution. The computational domain is $[-\pi,\pi]$, with the periodic boundary condition. The time step is taken as $\Delta t = 0.1\Delta x$. When the piecewise P^1 elements are used in the LDG method, the second order semi-implicit Runge-Kutta method is used for time integration, while for P^2 approximation, we adopt the third order scheme. The L^2 and L^∞ errors and the numerical orders of accuracy at time $T = 0.5$ are contained in Table 3.1, which shows $(k+1)$-th order of accuracy in both L^2 and L^∞ norms for P^k approximation.

To demonstrate the optimal complexity (with respect to the grid size Δx) of the multigrid solver, we provide evidence that the multigrid convergence rate is independent of Δx for P^1 and P^2 approximation, which is shown in Figure 3.1.

Table 3.1: Accuracy test for surface diffusion of graphs (3.10) with the exact solution (3.18) at time $T = 0.5$.

	N	L^2 error	order	L^∞ error	order
$\mathcal{P}^1$	16	7.31E-04	–	9.13E-04	–
	32	1.82E-04	2.00	2.30E-04	1.99
	64	4.56E-05	2.00	5.76E-05	2.00
	128	1.14E-05	2.00	1.44E-05	2.00
$\mathcal{P}^2$	16	2.29E-05	–	2.69E-05	–
	32	2.87E-06	3.00	3.40E-06	2.99
	64	3.59E-07	3.00	4.26E-07	3.00
	128	4.48E-08	3.00	5.62E-08	2.92

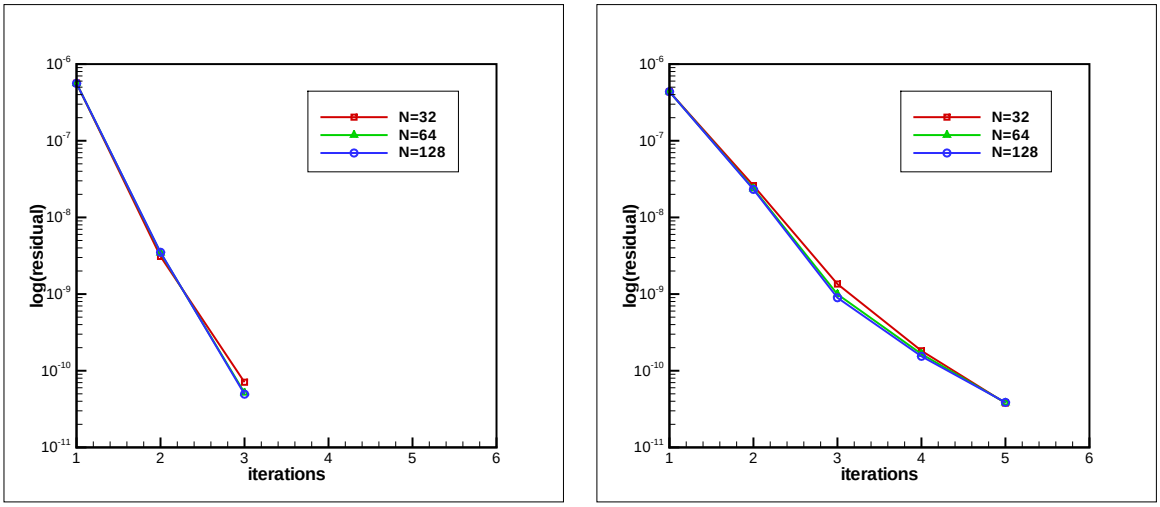

(a) $\mathcal{P}^1$ approximation

(b) $\mathcal{P}^2$ approximation

Figure 3.1: Convergence rates of multigrid solver with $\mathcal{P}^1$ and $\mathcal{P}^2$ approximation for surface diffusion of graphs.

Example 3.2. Positive perturbation for surface diffusion of graphs

In this example, we consider the numerical solutions of the two-dimensional surface diffusion of graphs (3.10) with the initial condition

$$u_0(x, y) = 1 + 0.3 \min(1, \max(0, 2 - 5\sqrt{x^2 + y^2})) \tag{3.19}$$

and periodic boundary conditions. The computational domain is $[-1, 1] \times [-1, 1]$. The P^2 elements with 64×64 cells and third order semi-implicit Runge-Kutta method are taken for space and time discretization, respectively. The numerical solutions at time $T = 0$, 0.0001,

0.001 and 0.005 are presented in Figure 3.2, which shows statistically similar patterns in the numerical solution as those in Xu and Shu [21], but with the advantage of taking larger time step ($\Delta t = O(\Delta x)$) comparing with the explicit time marching method ($\Delta t = O(\Delta x^4)$) in [21].

We present in Figure 3.3 the time evolution of the L^2 norm of the numerical solution and its dissipation, *i.e.*

$$\frac{d}{dt}E(t) = -I(t),$$

where the functional $E(t)$ and the dissipation $I(t)$ are defined by

$$E(t) = \frac{1}{2}\int_\Omega u^2(t,\boldsymbol{x})d\boldsymbol{x}, \qquad I(t) = \int_\Omega H^2(u(t,\boldsymbol{x}))d\boldsymbol{x}.$$

The results show that our numerical scheme is stable with a lager time step of ($\Delta t = O(\Delta x)$).

Example 3.3. Accuracy test for Willmore flow of graphs

In this example, we consider the accuracy test for one-dimensional Willmore flow of graphs. We test our scheme taking the exact solution

$$u(x,t) = 0.05\cos(t)\sin(x) \tag{3.20}$$

for equation (3.11) with a source term f, which is a given function so that (3.18) is the exact solution. The computational domain is $[-\pi,\pi]$, with the periodic boundary condition. The time step is taken as $\Delta t = 0.1\Delta x$. When the piecewise P^1 elements are used in the LDG method, the second order semi-implicit Runge-Kutta method is used for time integration, while for P^2 approximation, we adopt the third order scheme. The L^2 and L^∞ errors and the numerical orders of accuracy at time $T = 0.5$ are contained in Table 3.2, which shows $(k+1)$-th order of accuracy in both L^2 and L^∞ norms for P^k approximation. Figure 3.4 shows the optimal complexity of the multigrid solver for the Willmore flow of graphs.

Example 3.4. Sine perturbation for Willmore flow of graphs

In this example, we consider the numerical solutions of the two-dimensional Willmore flow of graphs (3.11) in the square domain $\Omega = [-2,2]\times[-2,2]$ with the initial condition

$$u_0(x,y) = 0.25\sin(\pi y)(0.25\sin(\pi x) + 0.5\sin(3\pi x)) \tag{3.21}$$

and periodic boundary condition. We use P^2 elements with 64×64 cells and third order semi-implicit Runge-Kutta method to solve equation (3.11). The numerical solutions at time $T = 0$, 0.0001, 0.001 and 0.01 are shown in Figure 3.5. With a larger time step

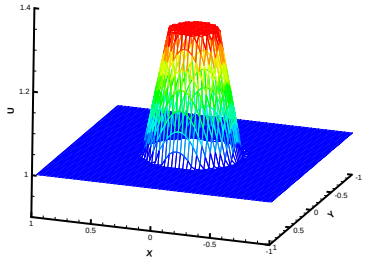

(a) $T = 0$

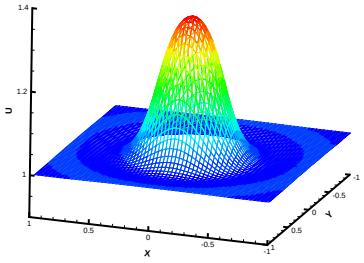

(b) $T = 0.0001$

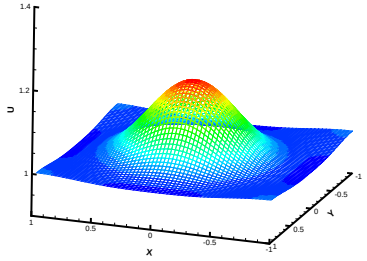

(c) $T = 0.001$

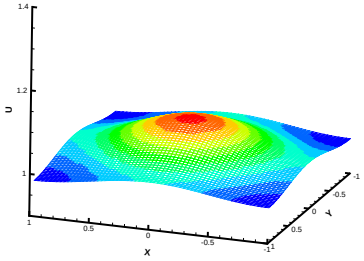

(d) $T = 0.005$

Figure 3.2: Numerical solutions for the surface diffusion of graphs with the initial condition (3.19).

of $\Delta t = O(\Delta x)$, our scheme gets the same results comparing the numerical calculations performed by Xu and Shu [21].

We present in Figure 3.6 the time evolution of the energy of the numerical solution and its dissipation, and the functional $E(t)$ and the dissipation $I(t)$ are defined by

$$E(t) = \frac{1}{2}\int_\Omega H^2(t,\boldsymbol{x})Q(t,\boldsymbol{x})d\boldsymbol{x}, \qquad I(t) = \int_\Omega \frac{(u(t,\boldsymbol{x}))^2}{Q(t,\boldsymbol{x})}d\boldsymbol{x}.$$

From Figure 3.6, we can see that our numerical scheme is stable numerically, *i.e.* the discrete energy is non-increasing about time.

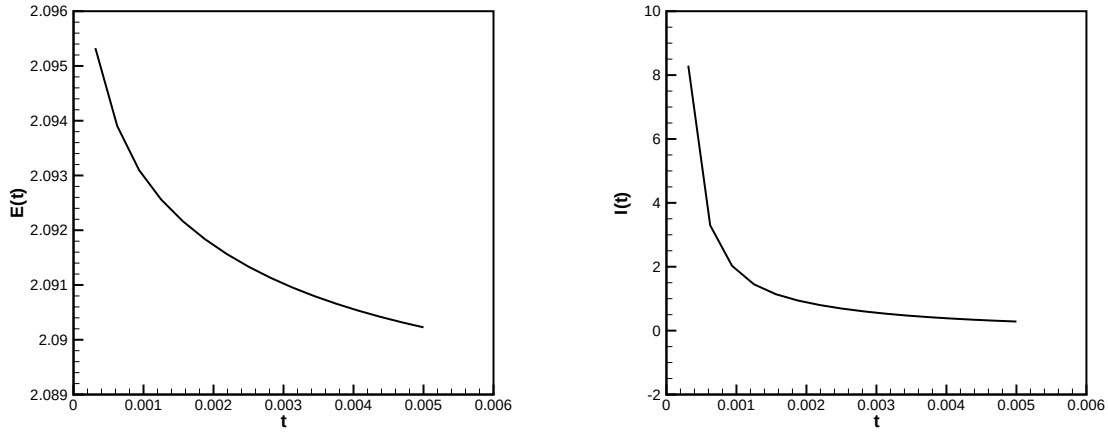

(a) functional $E(t)$ (b) dissipation $I(t)$

Figure 3.3: Evolution of the L^2 norm and the dissipation for surface diffusion of graphs

Table 3.2: Accuracy test for Willmore flow of graphs (3.11) with the exact solution (3.20) at time $T = 0.5$.

	N	L^2 error	order	L^∞ error	order
$\mathcal{P}^1$	16	7.31E-04	–	9.09E-04	–
	32	1.82E-04	2.00	2.28E-04	1.99
	64	4.56E-05	2.00	5.66E-05	2.00
	128	1.14E-05	2.00	1.39E-05	2.02
$\mathcal{P}^2$	16	2.29E-05	–	2.69E-05	–
	32	2.87E-06	3.00	3.40E-06	2.99
	64	3.59E-07	3.00	4.26E-07	2.99
	128	4.49E-08	3.00	5.42E-08	2.98

3.2 The Cahn-Hilliard equation

In this subsection, we consider LDG spatial discretization coupled with high order semi-implicit Runge-Kutta method (2.7)-(2.9) for the Cahn-Hilliard equation

$$u_t = \nabla \cdot (b(u)\nabla(-\gamma\Delta u + \Psi'(u))), \tag{3.22}$$

where $\Psi(u) = \frac{1}{4}(u^2 - 1)^2$, $b(u)$ is the degenerate mobility, and γ is a positive constant. Xia *et al.* [17] developed an LDG method for the Cahn-Hilliard equation and based on the consideration of high order in spatial derivative, Guo and Xu [11] constructed a semi-implicit

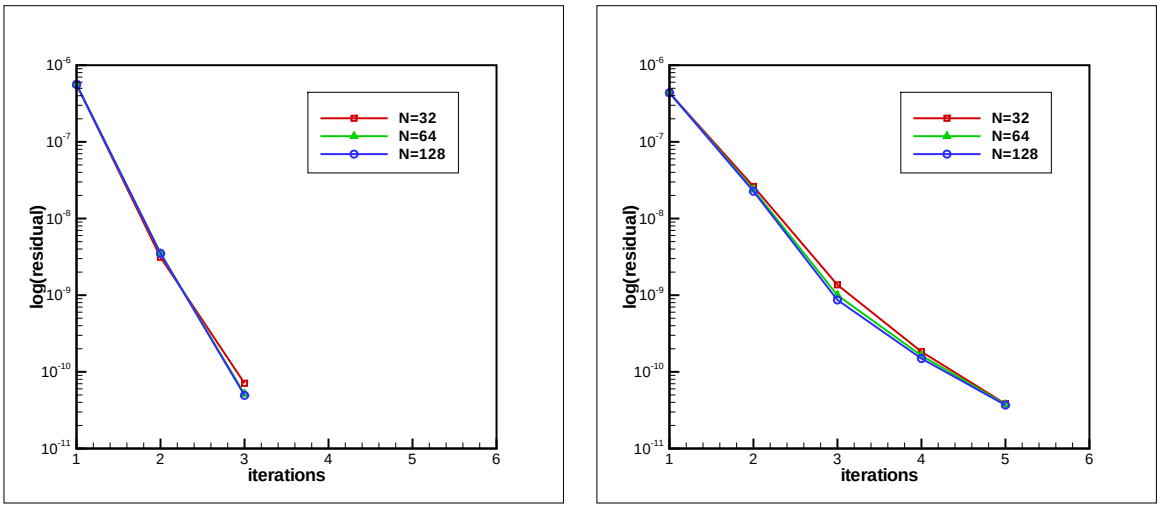

(a) $\mathcal{P}^1$ approximation (b) $\mathcal{P}^2$ approximation

Figure 3.4: Convergence rates of multigrid solver with $\mathcal{P}^1$ and $\mathcal{P}^2$ approximation for Willmore flow of graphs.

convex splitting scheme for equation (3.22). The convex splitting scheme was unconditionally stable with a first order temporal accuracy, and the additive Runge-Kutta method was adopted in [11] to achieve high order accuracy in time for Cahn-Hilliard equation with constant mobility, *i.e.* $b(u)$ is constant. While for Cahn-Hilliard equation with degenerate mobility, Guo and Xu introduced the linearization scheme and fully implicit scheme to achieve high order temporal accuracy, but the implementation was difficult and the constraint of time step was still hard for these two methods. It would therefore be desirable to develop high order semi-implicit time marching method to solve the Cahn-Hilliard equation with degenerate mobility.

The convex splitting which was proposed in [11] is given in the following form:

$$\frac{u^{n+1}-u^n}{\Delta t} = \nabla \cdot (b(u^n)\nabla(-\gamma\Delta u^{n+1} + (u^{n+1})^3 - u^n)). \tag{3.23}$$

Based on the unconditionally stable convex splitting scheme (3.23), and to apply our semi-implicit Runge-Kutta scheme, we rewrite the Cahn-Hilliard equation in the form of (2.1) with u the component treated explicitly, v the component treated implicitly, and

$$\mathcal{H}(t,u,v) = \nabla \cdot (b(u)\nabla(-\gamma\Delta v + v^3 - u)). \tag{3.24}$$

Then we will get a stable semi-implicit scheme for the Cahn-Hilliard equation, which is high order accurate in both space and time.

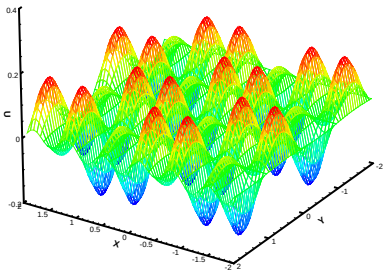

(a) $T = 0$

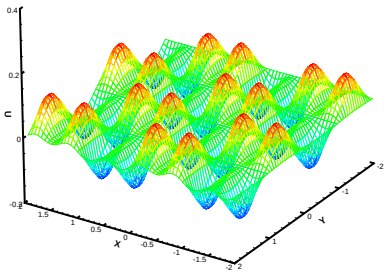

(b) $T = 0.0001$

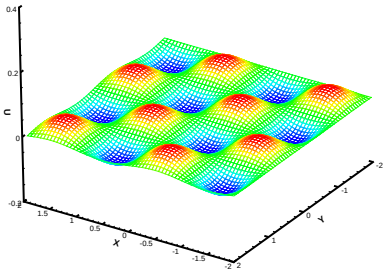

(c) $T = 0.001$

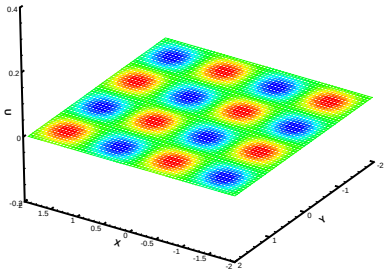

(d) $T = 0.01$

Figure 3.5: Numerical solutions for the Willmore flow of graphs with the initial condition (3.21).

Example 3.5. Accuracy test for Cahn-Hilliard equation

We consider the Cahn-Hilliard equation (3.22) with $b(u) = 1 - u^2$, $\gamma = 1$ in the domain $\Omega = [-\pi, \pi]$ and with periodic boundary condition. We test our method taking the exact solution

$$u(x,t) = e^{-t}\sin(x) \tag{3.25}$$

for equation (3.22) with a source term f, which is a given function so that make the exact solution (3.25). The time step is taken as $\Delta t = 0.1\Delta x$. When the piecewise P^1 elements are

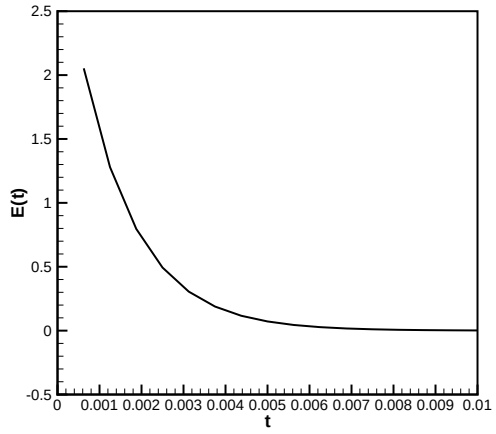

(a) functional $E(t)$

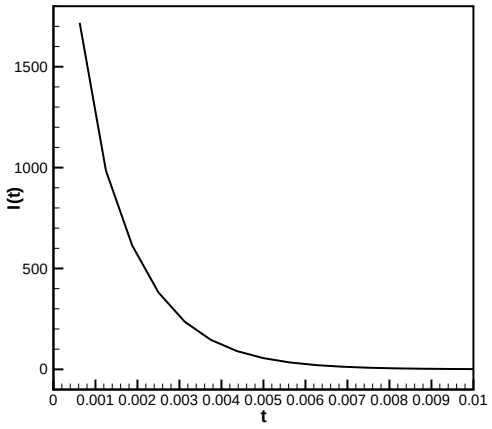

(b) dissipation $I(t)$

Figure 3.6: Evolution of the energy and the dissipation for Willmore flow of graphs

used in the LDG method, the second order semi-implicit Runge-Kutta method is used for time integration, while for P^2 approximation, we adopt the third order scheme. Table 3.3 presents the L^2 and L^∞ errors and the numerical orders of accuracy at time $T = 0.5$, which shows $(k+1)$-th order of accuracy in both L^2 and L^∞ norms for P^k approximation with larger time step comparing numerical methods in [17]. Figure 3.7 presents the optimal complexity of the multigrid solver for the Cahn-Hilliard equation, which shows that the convergence in independent of the grid size Δx.

Table 3.3: Accuracy test for the Cahn-Hilliard equation (3.22) with the exact solution (3.25) at time $T = 0.5$.

	N	L^2 error	order	L^∞ error	order
$\mathcal{P}^1$	16	1.01E-02	–	1.26E-02	–
	32	2.52E-03	2.00	3.16E-03	2.00
	64	6.31E-04	2.00	7.89E-04	2.00
	128	1.57E-04	2.00	1.96E-04	2.00
$\mathcal{P}^2$	16	3.18E-04	–	3.75E-04	–
	32	3.98E-05	3.00	4.72E-05	2.99
	64	5.00E-06	2.99	5.98E-06	2.98
	128	6.27E-07	3.00	7.54E-07	2.99

Example 3.6. Long time simulation for Cahn-Hilliard equation

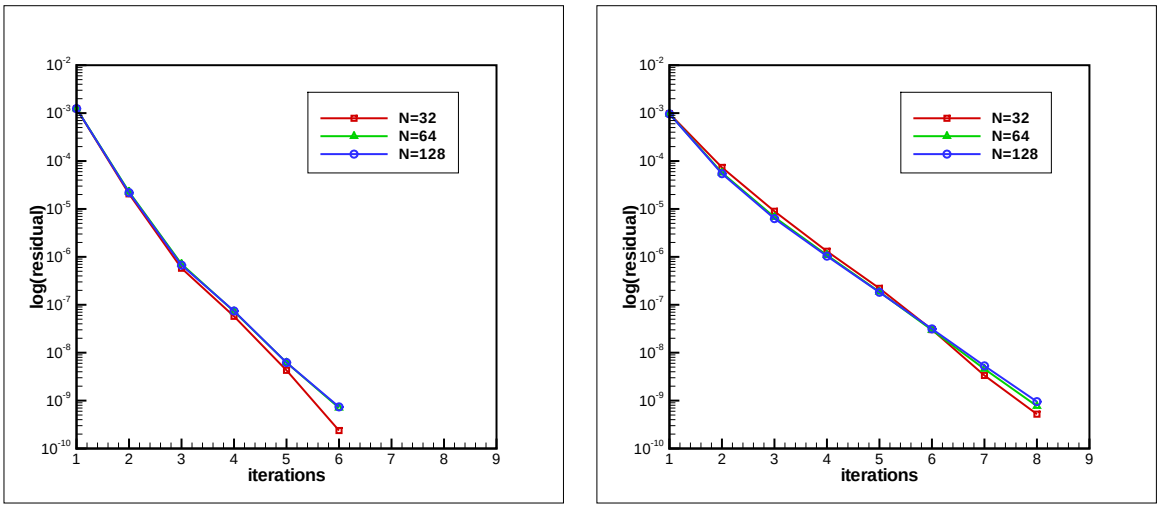

(a) $\mathcal{P}^1$ approximation (b) $\mathcal{P}^2$ approximation

Figure 3.7: Convergence rates of multigrid solver with $\mathcal{P}^1$ and $\mathcal{P}^2$ approximation for Cahn-Hilliard equation.

In the square domain $\Omega = [0, 6.4] \times [0, 6.4]$, we consider the Cahn-Hilliard equation (3.22) with

$$\Psi'(u) = u^3 - u, \quad b(u) = \sqrt{(1+u)^2(1-u)^2 + \gamma}, \quad \gamma = 0.001, \tag{3.26}$$

and Neumann boundary condition, *i.e.*

$$\frac{\partial u}{\partial \boldsymbol{\nu}} = b(u)\nabla(-\gamma\Delta u + \Psi'(u)) \cdot \boldsymbol{\nu} = 0, \quad \text{on } \partial\Omega. \tag{3.27}$$

The initial data is a random field of values that are uniformly distributed about the average composition $\bar{u} = -0.05$, with amplitude 0.05.

We use the P^2 element and third order semi-implicit Runge-Kutta method (3.24), which is based on the convex splitting scheme proposed in [11]. Figure 3.8 shows the contour lines of the numerical solution in some selected time levels. We present in Figure 3.9 the time evolution of the discrete energy of the numerical solution and its dissipation, *i.e.*

$$\frac{d}{dt}E(t) = -I(t),$$

where the functional $E(t)$ and the dissipation are given by the following form

$$E(t) = \int_\Omega \left(\frac{\gamma}{2}|\nabla u|^2 + \Psi(u)\right) d\boldsymbol{x}, \qquad I(t) = \int_\Omega b(u)|\nabla \mu|^2 d\boldsymbol{x},$$

with $\mu = -\gamma\Delta u + \Psi'(u)$. The results show that our numerical scheme is stable.

This long time simulation example shows the capability of the LDG method, the high order semi-implicit temporal method and the multigrid solver for solving the Cahn-Hilliard equation with degenerate mobility.

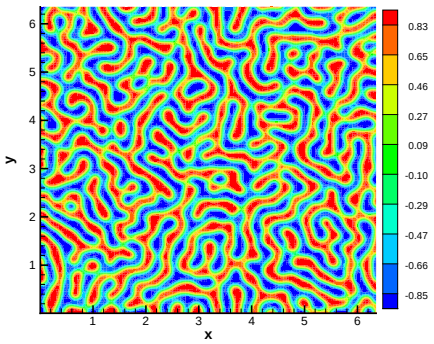

(a) $T = 0.1$

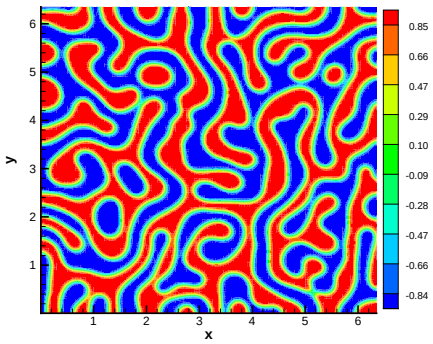

(b) $T = 1$

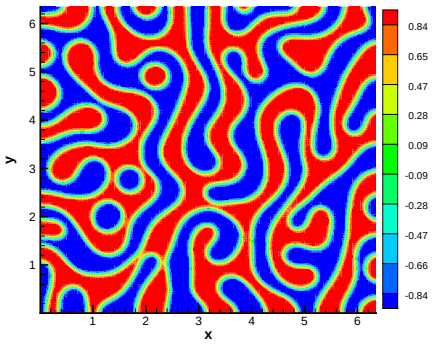

(c) $T = 3$

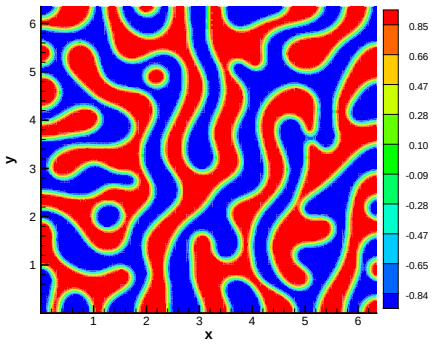

(d) $T = 5$

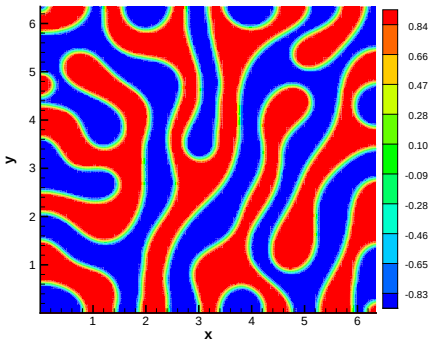

(e) $T = 15$

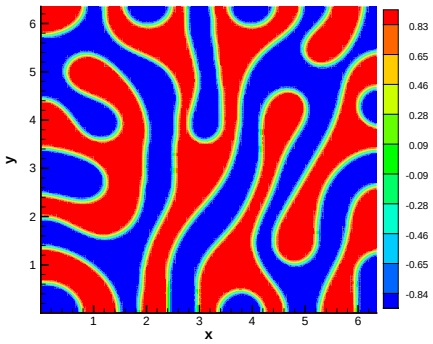

(f) $T = 30$

Figure 3.8: The time evolution of the Cahn-Hilliard equation with $\mathcal{P}^2$ approximation on a 128×128 mesh.

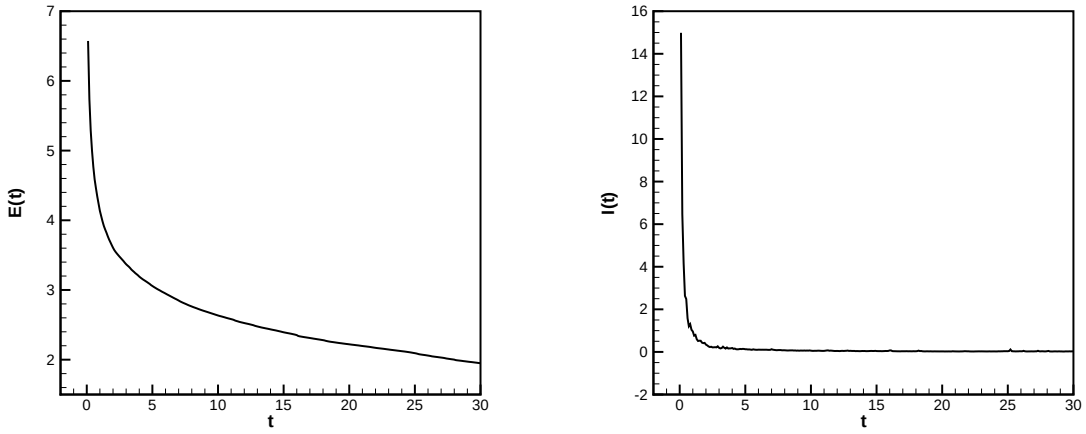

(a) functional $E(t)$ (b) dissipation $I(t)$

Figure 3.9: Evolution of the energy and the dissipation for Cahn-Hilliard equation

3.3 The Allen-Cahn/Cahn-Hilliard system

In this subsection, we consider LDG spatial discretization coupled with high order semi-implicit time marching methods for the Allen-Cahn/Cahn-Hilliard system

$$\begin{cases} u_t = \nabla \cdot [b(u,v)\nabla(\Psi_u(u,v) - \gamma\Delta u)], \\ \rho v_t = -b(u,v)[\Psi_v(u,v) - \gamma\Delta v], \end{cases} \tag{3.28}$$

where the degenerate mobility is

$$b(u,v) = u(1-u)(\frac{1}{4} - v^2), \tag{3.29}$$

and the homogeneous free energy $\Psi(u,v)$ is

$$\Psi(u,v) = \theta[\Phi(u+v) + \Phi(u-v)] + \frac{1}{2}[\alpha u(1-u) - \beta v^2], \tag{3.30}$$

$$\Phi(s) = s\ln s + (1-s)\ln(1-s). \tag{3.31}$$

Here θ represents the temperature, γ is the coefficient of gradient energy and α, β are the coefficients of nearest and next-nearest pairwise energetic interactions. Xia *et al.* [19] developed an LDG method for the system (3.28), and in which an explicit time marching method was employed. However, the explicit method was not efficient because of its severe time step restriction ($\Delta t = O(\Delta x^4)$) for stability, especially for long time simulations. It would therefore be desirable to develop high order semi-implicit time marching methods to relax the severe time step restriction.

3.3.1 The spectral deferred correction method

For the Allen-Cahn/Cahn-Hilliard system with constant mobility, *i.e.* $b(u, v)$ is constant, a first order semi-implicit time discretization method can be given as follows:

$$\begin{cases} \dfrac{u^{n+1} - u^n}{\Delta t} = \nabla \cdot [\nabla(\Psi_u(u^n, v^n) - \gamma \Delta u^{n+1})], \\ \rho \dfrac{v^{n+1} - v^n}{\Delta t} = -[\Psi_v(u^n, v^n) - \gamma \Delta v^{n+1}], \end{cases} \tag{3.32}$$

which treating the stiff term implicitly and the non-stiff term explicitly. The scheme is only first order accurate in time. To improve the temporal accuracy, we can apply the semi-implicit SDC method based on the first order scheme (3.32). An advantage of the SDC method is that it is a one step method and can be constructed easily and systematically for any order of accuracy. For convenience, the first order scheme (3.32) can be rewritten as

$$\begin{cases} u^{n+1} = u^n + \Delta t(F_S(u^{n+1}) + F_N(u^n, v^n)), \\ v^{n+1} = v^n + \Delta t(G_S(v^{n+1}) + G_N(u^n, v^n)), \end{cases} \tag{3.33}$$

where F_S, G_S represent the linearly implicit part and F_N, G_N represent the nonlinearly explicit part of the semi-implicit first order scheme, which means

$$\begin{cases} F_S(u) = -\gamma \Delta^2 u, \qquad F_N(u, v) = \Delta(\Psi_u(u, v)), \\ G_S(v) = \gamma \Delta v, \qquad G_N(u, v) = -\Psi_v(u, v). \end{cases} \tag{3.34}$$

Then the semi-implicit SDC method can be applied iteratively to achieve high order temporal accuracy. For a detailed description of the SDC method as well as their implementation and applications, we refer the readers to [9, 13, 18, 20].

3.3.2 The high order semi-implicit Runge-Kutta method

For the Allen-Cahn/Cahn-Hilliard system with degenerate mobility, *i.e.* $b(u, v)$ is not constant, we know that the stiff and non-stiff components can not be well separated. In this case, the semi-implicit SDC method is not efficient any more. Therefore, we adopt the high order semi-implicit Runge-Kutta method. And to apply our semi-implicit scheme (2.7)-(2.9), we write the Allen-Cahn/Cahn-Hilliard system (3.28) in the form of (2.1) with $u = (u_1, u_2)$ the component treated explicitly, $v = (v_1, v_2)$ the component treated implicitly and

$$\mathcal{H}(t, u, v) = \begin{cases} \nabla \cdot [b(u_1, u_2)\nabla(\Psi_u(u_1, u_2) - \gamma \Delta v_1)], \\ -\dfrac{1}{\rho} b(u_1, u_2)[\Psi_v(u_1, u_2) - \gamma \Delta v_2]. \end{cases} \tag{3.35}$$

The semi-implicit scheme is high order accurate in time and expected to be stable with a larger time step comparing with explicit methods, which is very efficient, especially for long time simulations in multi-dimensional case.

Example 3.7. We consider the Allen-Cahn/Cahn-Hilliard system (3.28) with $\Psi(u,v) = u - u^2 - \frac{1}{2}v^2$, $b(u,v) = (1+u^2)(1+v^2)$ in the domain $\Omega = [0, 4\pi]$ and with periodic boundary condition. We test our method taking the exact solution

$$u(x,t) = e^{-0.5t}\sin(x), \qquad v(x,t) = e^{-t}\cos(0.5x) \tag{3.36}$$

for equation (3.28) with a source term f, which is a given function so that (3.36) is the exact solution. When the piecewise P^1 elements are used in the LDG method, the second order semi-implicit Runge-Kutta method is used for time integration, while for P^2 approximation, we adopt the third order scheme. The L^2 and L^∞ errors and the numerical orders of accuracy at time $T = 0.5$ are contained in Table 3.4, which shows the $(k+1)$-th order of accuracy in both L^2 and L^∞ norms for P^k approximation. Figure 3.10 shows the near optimal complexity of the multigrid solver for the Allen-Cahn/Cahn-Hilliard system, which means that the convergence is nearly independent of the grid size Δx.

Table 3.4: Accuracy test for the Allen-Cahn/Cahn-Hilliard system (3.28) with the exact solution (3.36) at time $T = 0.5$.

		u				v			
	N	L^2 error	order	L^∞ error	order	L^2 error	order	L^∞ error	order
$\mathcal{P}^1$	16	7.61E-02	–	5.82E-02	–	1.91E-02	–	9.79E-03	–
	32	1.85E-02	2.03	1.57E-02	1.89	4.28E-03	2.16	2.39E-03	2.03
	64	4.59E-03	2.01	3.99E-03	1.98	1.03E-03	2.04	6.12E-04	1.96
	128	1.14E-03	2.00	1.00E-03	2.00	2.57E-04	2.01	1.53E-04	1.99
$\mathcal{P}^2$	16	4.70E-03	–	4.13E-03	–	5.77E-04	–	3.84E-04	–
	32	5.80E-04	3.01	4.91E-04	3.07	7.54E-05	2.93	4.84E-05	2.99
	64	7.27E-05	2.99	6.14E-05	2.99	1.02E-05	2.87	6.27E-06	2.94
	128	9.38E-06	2.96	7.94E-06	2.95	1.53E-06	2.74	8.56E-07	2.87

Example 3.8. We consider the Allen-Cahn/Cahn-Hilliard system (3.28) in $\Omega = [0,1]\times[0,1]$, $\gamma = 5 \times 10^{-3}$, $\theta = 0.1$ with degenerate and constant mobility respectively. The initial

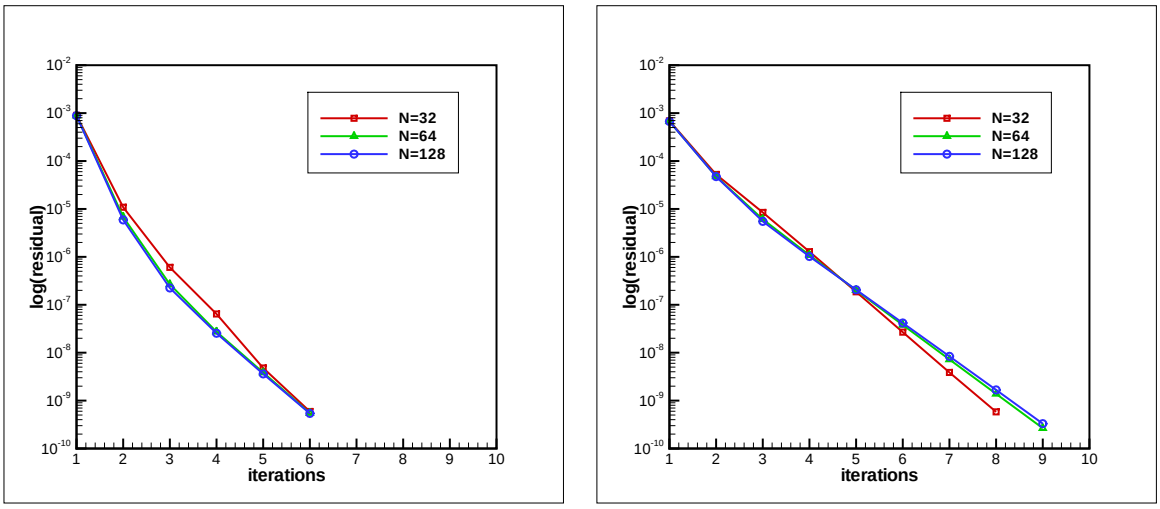

(a) $\mathcal{P}^1$ approximation (b) $\mathcal{P}^2$ approximation

Figure 3.10: Convergence rates of multigrid solver with $\mathcal{P}^1$ and $\mathcal{P}^2$ approximation for Allen-Cahn/Cahn-Hilliard system.

condition $(u^0, v^0) = (0.55+\delta_u, \delta_v)$, where δ_u, δ_v are random with $\max(||\delta_u||_\infty, ||\delta_v||_\infty) \leq 0.05$. Neumann boundary conditions are prescribed, *i.e.*

$$\frac{\partial u}{\partial \boldsymbol{\nu}} = \frac{\partial v}{\partial \boldsymbol{\nu}} = b(u,v)\nabla(-\gamma\Delta u + \Psi_u(u,v)) \cdot \boldsymbol{\nu} = 0, \quad \text{on } \partial\Omega. \tag{3.37}$$

We consider the following cases:

1. $\alpha = 2$, $\beta = 4$, $\rho = 0.08$ with degenerate mobility (3.29),
2. $\alpha = 2$, $\beta = 4$, $\rho = 0.08$ with constant mobility $b = \frac{1}{16}$, which is the maximum of the degenerate mobility.

The computational parameters are the spatial discretization cell size $\Delta x = 1/N$ with $N = 64$ and the piecewise P^k polynomial basis with $k = 2$. For the Allen-Cahn/Cahn-Hilliard system with degenerate mobility, the third order semi-implicit Runge-Kutta method is employed, while for constant mobility case, we apply the third order semi-implicit SDC time temporal method.

The numerical results for degenerate mobility and constant mobility are given in Figure 3.11 and Figure 3.12, respectively. We can see that the solution with degenerate mobility (3.29) changes more slowly than the solution with constant mobility, which is the maximum of the degenerate mobility.

We present in Figure 3.13 the time evolution of the energy of the numerical solution and its dissipation , and the functional $E(t)$ and dissipation $I(t)$ are defined by

$$E(t) = \int_\Omega \left(\frac{\gamma}{2}(|\nabla u|^2 + |\nabla v|^2) + \Psi(u,v) \right) d\boldsymbol{x}, \qquad I(t) = \int_\Omega b(u,v) \left(|\nabla \mu_1|^2 + \frac{1}{\rho}(\mu_2)^2 \right) d\boldsymbol{x},$$

with $\mu_1 = -\gamma \Delta u + \Psi_u$ and $\mu_2 = -\gamma \Delta v + \Psi_v$, which shows that our numerical schemes are stable.

4 Conclusion

In this paper, we have explored a high order semi-implicit Runge-Kutta method for solving the ODEs resulting from a local discontinuous Galerkin spatial discretization to highly nonlinear PDEs containing higher order spatial derivatives, which consist of the surface diffusion and Willmore flow of graphs, the Cahn-Hilliard equation and the Allen-Cahn/Cahn-Hilliard system. With the proposed semi-implicit temporal method, the severe time step restriction of explicit methods can be relaxed and we can achieve high order temporal accuracy with a larger time step. However, the equations at the implicit time level are linear or nonlinear, and to enhance the efficiency of the solver, we employed the linear and nonlinear multigrid solver to solve algebraic equations, respectively. Numerically we show the high order accuracy of the proposed schemes, in both time and space, with a larger time step. Also, the long time simulations show the capacity and efficiency of the proposed temporal and spatial methods.

References

[1] F. Bassi and S. Rebay, *A high-order accurate discontinuous finite element method for the numerical solution of the compressible Navier-Stokes equations*, J. Comput. Phys., **131**, (1997), pp.267-279.

[2] S. Boscarino, F. Filbet and G. Russo, *High order semi-implicit schemes for time dependent partial differential equations*, submitted.

[3] B. Cockburn and C.-W. Shu, *TVB Runge-Kutta local projection discontinuous Galerkin finite element method for conservation laws II: general framework*, Math. Comp., **52**, (1989), pp.411-435.

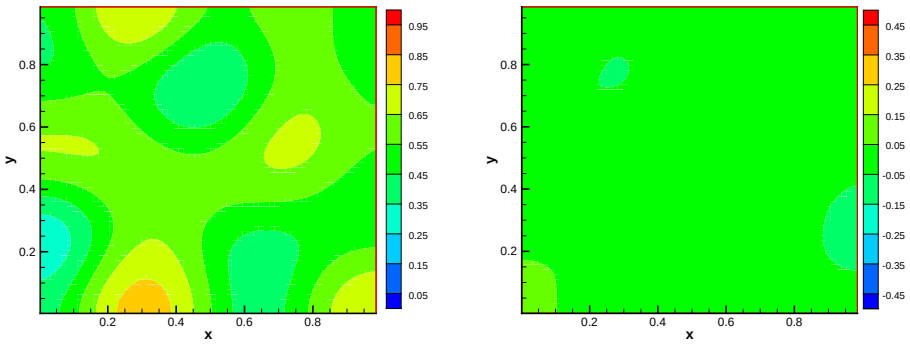

(a) $u, T = 1$

(b) $v, T = 1$

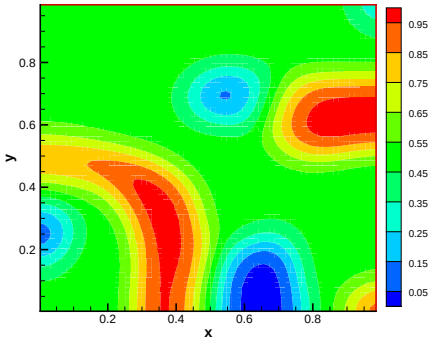

(c) $u, T = 4$

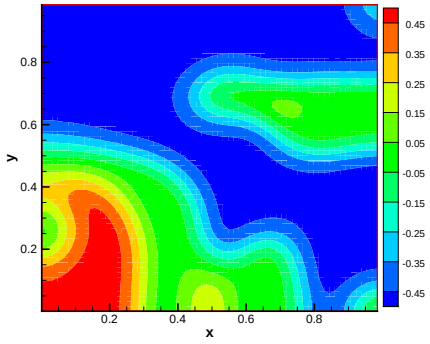

(d) $v, T = 4$

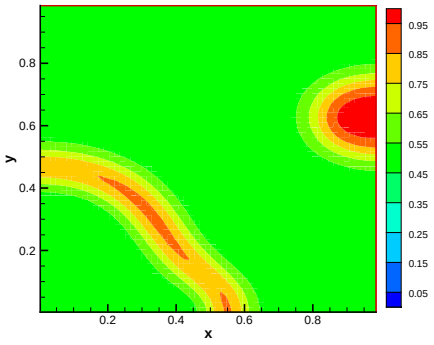

(e) $u, T = 8$

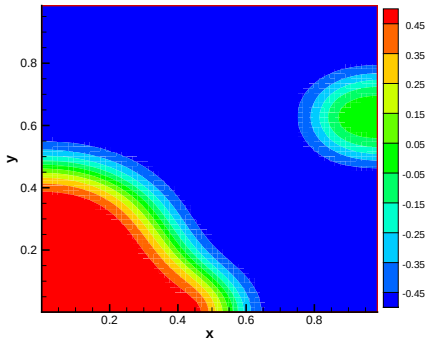

(f) $v, T = 8$

Figure 3.11: The time evolution of the Allen-Cahn/Cahn-Hilliard system with degenerate mobility (3.29). $\mathcal{P}^2$ approximation on a 64×64 mesh.

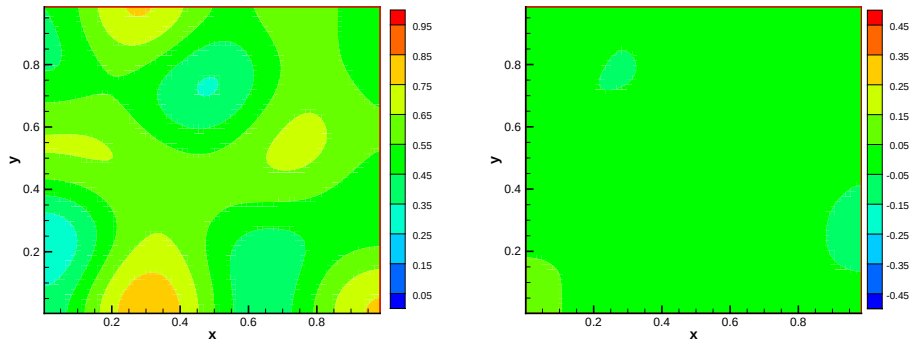

(a) $u, T = 1$ (b) $v, T = 1$

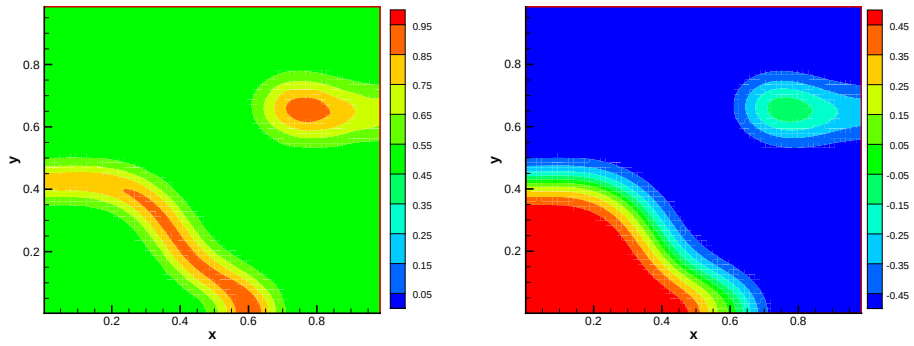

(c) $u, T = 4$ (d) $v, T = 4$

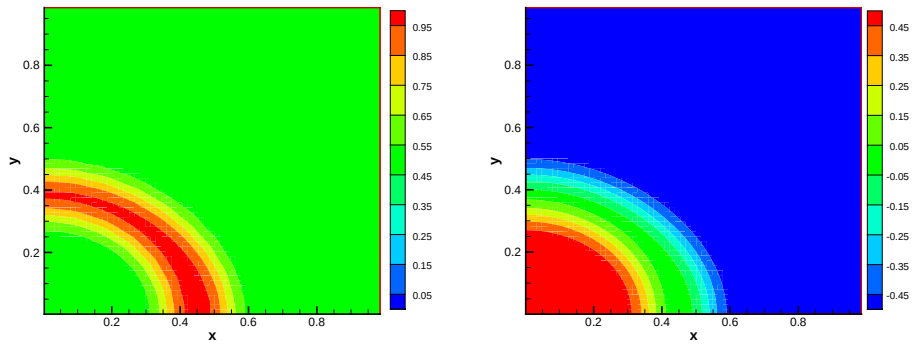

(e) $u, T = 8$ (f) $v, T = 8$

Figure 3.12: The time evolution of the Allen-Cahn/Cahn-Hilliard system with constant mobility $b = 1/16$. $\mathcal{P}^2$ approximation on a 64×64 mesh.

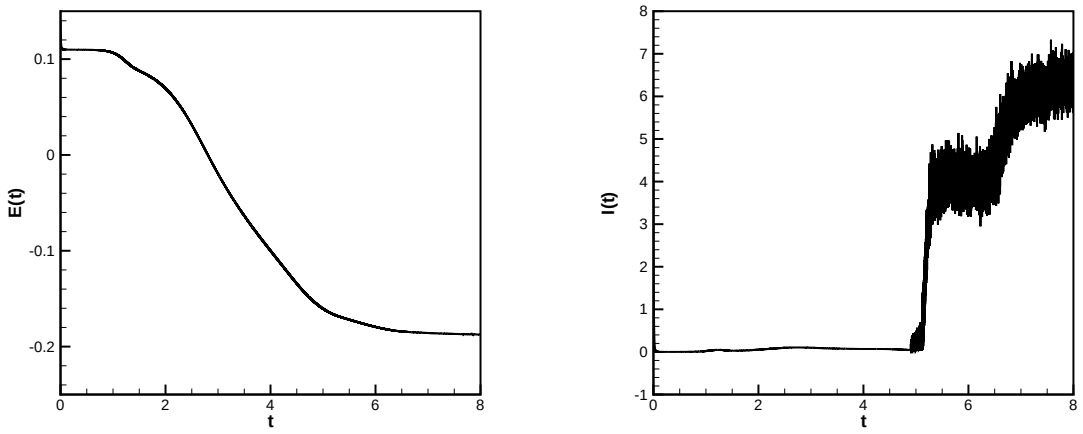

(a) functional $E(t)$ (b) dissipation $I(t)$

Figure 3.13: Evolution of the energy and the dissipation for Allen-Cahn/Cahn-Hilliard system.

[4] B. Cockburn, S.-Y. Lin and C.-W. Shu, *TVB Runge-Kutta local projection discontinuous Galerkin finite element method for conservation laws III: one dimensional systems*, J. Comput. Phys., **84**, (1989), pp.90-113.

[5] B. Cockburn, S. Hou and C.-W. Shu, *The Runge-Kutta local projection discontinuous Galerkin finite element method for conservation laws IV: the multidimensional case*, Math. Comp., **54**, (1990), pp.545-581.

[6] B. Cockburn and C.-W. Shu, *The Runge-Kutta discontinuous Galerkin method for conservation laws V: multidimensional systems*, J. Comput. Phys., **141**, (1998), pp.199-224.

[7] B. Cockburn and C.-W. Shu, *The local discontinuous Galerkin method for time-dependent convection-diffusion systems*, SIAM J. Numer. Anal., **35**, (1998), pp.2440-2463.

[8] K. Deckelnick and G. Dziuk, *Error analysis of a finite element method for the Willmore flow of graphs*, Interfaces Free Bound., **8**, (2006), pp.21-46.

[9] A. Dutt, L. Greengard and V. Rokhlin, *Spectral deferred correction methods for ordinary differential equations*, BIT, **40**, (2000), pp.241-266.

[10] D.J. Eyre, *Unconditionally gradient stable time marching the Cahn-Hilliard equation*, in: J.W. Bullard, R. Kalia, M. Stoneham, L.Q. Chen (Eds), Computational and Mathe-

matical Models of Microstructural Evolution, vol. 53, Materials Research Society, Warrendale, 1998, pp.1685-1712.

[11] R. Guo and Y. Xu, *Efficient solvers of discontinuous Galerkin discretization for the Cahn-Hilliard equations*, J. Sci. Comput., **58**, (2014), pp.380-408.

[12] E. Hairer and G. Wanner, *Solving Ordinary Differential Equation. II. Stiff and differential algebraic problems*, Springer Series in Comput. Mathematics, Vol. 14, Springer Verlag, (2nd edition), 1996.

[13] M.L. Minion,*Semi-implicit spectral deferred correction methods for ordinary differential equations*, Math. Sci., **1**, (2003), pp.471-500.

[14] W.H. Reed and T.R. Hill, *Triangular mesh method for the neutron transport equation*, Technical report LA-UR-73-479, Los Alamos Scientific Laboratory, Los Alamos, NM, 1973.

[15] P. Smereka, *Semi-implicit level set methods for curvature and surface diffusion motion*, J. Sci. Comput., **19**, (2003), pp.439-456.

[16] U. Trottenberg, C. Oosterlee and A. Schüller, *Multigrid*, Academic Press, New York (2005).

[17] Y. Xia, Y. Xu and C.-W. Shu, *Local discontinuous Galerkin methods for the Cahn-Hilliard type equations*, J. Comput. Phys., **227**, (2007), pp.677-693.

[18] Y. Xia, Y. Xu and C.-W. Shu, *Efficient time discretization for local discontinuous Galerkin methods*, Discrete Contin. Dyn. Syst. Ser. B, **8**, (2007), pp.677-693.

[19] Y. Xia, Y. Xu and C.-W. Shu, *Application of the local discontinuous Galerkin method for the Allen-Cahn/Cahn-Hilliard system*, Commun. Comput. Phys., **5**, (2009), pp.821-835.

[20] Y. Xia, *A fully discrete stable discontinuous Galerkin method for the thin film epitaxy problem without slope selection*, J. Comput. Phys., **280**, (2015), pp.248-260.

[21] Y. Xu and C.-W. Shu, *Local discontinuous Galerkin method for surface diffusion and Willmore flow of graphs*, J. Sci. Comput., **40**, (2009), pp.375-390.

[22] Y. Xu and C.-W. Shu, *Local discontinuous Galerkin methods for high-order time-dependent partial differential equations*, Commun. Comput. Phys., **7**, (2010), pp.1-46.